The oscillations of a small floating bubble

N. Q. Lu, H. N. Oguz, and A. Prosperetti
Department of Mechanical Engineering, The Johns Hopkins University, Baltimore, Maryland 21218

(Received 13 June 1988; accepted 4 October 1988)

A simple model of a small bubble floating at the surface of a liquid before bursting is considered. The oscillations of this system are studied by means of a Lagrangian method. It is found that two fundamentally different modes exist. The *surface mode* has low frequency and does not change appreciably the volume of the immersed part of the bubble: As a consequence, its efficiency as a source of sound in the water is very limited. The *volume mode* has a much higher frequency and is a more efficient radiator in the water, although it may be hard to excite. Both modes behave as monopole sources in the air. It is therefore predicted that an oscillating floating bubble is a much more intense source of sound in the air than in the liquid. This conclusion seems to be supported by experimental observations.

I. INTRODUCTION

When a small gas bubble rises to the surface of a liquid it does not burst immediately, but rather only after some time which, depending on the degree of contamination of the liquid surfaces and other factors,[1–4] can range widely from a fraction of a second to hours. This time is necessary for the liquid film covering the top of the bubble to evaporate and drain under the effect of gravity and surface tension, thinning enough that molecular forces can cause its instability and rupture.[5,6] During this period the bubble can be considered in a sort of equilibrium state and is capable of executing volume and shape oscillations. For example, Pumphrey[7] has observed noise produced in the air when two such floating bubbles coalesce and the resulting excess surface energy causes them to oscillate. This coalescence process is not purely the fruit of random encounters since neighboring floating bubbles attract each other.[8] Indeed, the liquid surface is lifted by the buoyancy force acting on the bubble (Fig. 1) and a neighboring bubble is induced by its own buoyancy to slide along this raised surface toward the first bubble. It can therefore be expected that the observed coalescence and oscillation of surface bubbles is a frequent process whenever gas rises to the surface of a liquid in the form of small bubbles: It can contribute to the sound produced in the air in these conditions, although little sound appears to be radiated in the water by this process,[7] a conclusion supported by the results of this study. Furthermore, these oscillations must have an effect on the draining of the film and its stability: They will therefore have an influence on the minute droplets to which the rupture of the film gives rise, which have a well-known geophysical significance,[9,10] and possibly on other processes such as the stability of foams.

In this paper we try to elucidate the basic physical features of the oscillations of a small floating bubble by means of a simple model. The simplifications introduced are rather crude, but the essence of the phenomenon seems to be captured nonetheless.

II. DIMENSIONAL CONSIDERATIONS

Before attempting to give a fuller quantitative description, it is useful to consider the problem in general terms. The parameters characterizing the liquid are its density ρ and surface tension σ. The bubble may be characterized by some linear dimension R, to be defined more precisely below, and by its stiffness, which is essentially its internal pressure p_G. In addition, the gravity g will play a role. With these elements one can construct three quantities having the dimensions of a frequency, namely,

$$\omega^2 = \sigma/\rho R^3, \tag{1}$$

$$\omega_V^2 = p_G/\rho R^2, \tag{2}$$

and

$$\omega_g^2 = g/R. \tag{3}$$

Equation (1) has the order of magnitude of the frequency of a bubble executing volume-preserving shape oscillations[11,12]; Eq. (2) is of the order of the pulsation frequency of a spherical bubble in volume oscillations,[12] and Eq. (3) is the frequency of gravity waves of wavelength R. If the ω_j, $j = 1,2,...$, denote the frequencies of the normal modes of oscillation of the floating bubble, dimensional analysis leads to relationships of the form

$$\omega_j = \omega \Psi_j(\omega/\omega_V, \omega/\omega_g). \tag{4}$$

Ordinarily, dimensional analysis would not enable one to go beyond this statement. However, if we restrict our considerations to small bubbles, gravity cannot play an important role and the second argument in (4) can be dropped. Furthermore, the first argument in (4) is normally very small. For example, for $R = 1$ mm, $p_G = 1$ atm, and $\sigma = 70$ erg/

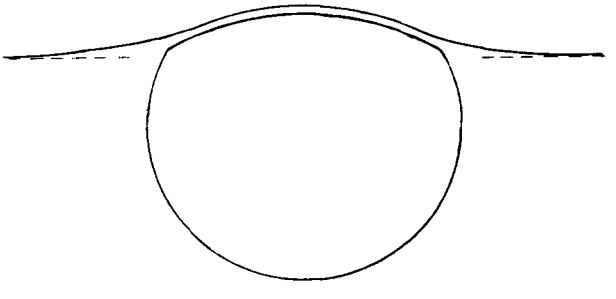

FIG. 1. Schematic shape of a floating bubble.

 0899-8213/89/020252-09$01.90

cm^2, we find $\omega/\omega_V \simeq 0.026$. Exploiting this fact, we can extract further information from (4). If the limit $\omega/\omega_V \to 0$ is approached by taking the bubble stiffness p_G larger and larger, (4) can give a meaningful result only if one of the functions Ψ_j, Ψ_1, say, is such that $\Psi_1(X) \to$ const as $X \to 0$. We therefore expect to have a mode such that

$$\omega_1 \sim \omega. \tag{5}$$

If now the same limit $\omega/\omega_V \to 0$ is approached by taking a smaller and smaller surface tension, $\omega_1 \to 0$ and Eq. (4) can only give a nontrival result if another Ψ_j exists, say Ψ_2, such that $\Psi_2(X) \sim 1/X$ as $X \to 0$. In this case we find a mode with a frequency

$$\omega_2 \sim \omega_V. \tag{6}$$

Equations (5) and (6) are expected to give the two dominant oscillation frequencies for small bubbles. The fact that the bubble stiffness does not affect the first mode [Eq. (5)] implies that the volume of a bubble oscillating according to this mode remains essentially constant. For the second mode [Eq. (6)] we cannot make an analogous statement concerning the surface area because, in the presence of an appreciable volume change, the energy $p\,dV$ associated to it is so large as to dominate any reasonable variation of the area.

We can now proceed to render these statements more precisely on the basis of a simple model.

III. MODEL

The actual shape of a floating bubble is determined by the complex interplay of gas pressure, surface tension, and gravity.[13] A simplified model of this configuration as used in the past[8] is shown in Fig. 1. We will simplify this model even further, as shown in Fig. 2, which also introduces some nomenclature used in the following. It will be seen that this procedure requires the introduction of additional, fictitious forces to push the bubble down. Our results will be applicable to the real (or, at any rate, more realistic) configuration of Fig. 1 only insofar as these forces are small. One expects this to happen for small bubbles, which are but slightly affected by buoyancy; this conclusion is indeed borne out by the results.

We take the gas volume to be bounded by two spherical segments of radius R and αR. The center of the immersed spherical segment is at a distance h from the plane free surface, reckoned negative below and positive above the surface. The center of the other spherical segment is at a distance H from the surface given by

$$H = [(\alpha^2 - 1)R^2 + h^2]^{1/2}, \tag{7}$$

as follows from elementary geometrical considerations. We shall use a Lagrangian approach in which R, h, and α are the generalized coordinates specifying the system's configuration. In terms of these quantities we write a Lagrangian $\mathscr{L}$ in the form

$$\mathscr{L} = \mathscr{T}(R,h,\dot{R},\dot{h}) - \mathscr{U}(R,h,\alpha). \tag{8}$$

The coordinate α enters into the potential energy $\mathscr{U}$ but, as will be seen, not in the kinetic energy $\mathscr{T}$. We shall calculate these quantities to second order in the perturbation of equilibrium, so that our theory is in fact a linear theory of the process under consideration.

In order to keep the problem as simple as possible we wish to disregard the surface ripples produced by the oscillating bubble as well as all the other damping mechanisms, which include thermal, viscous, and acoustic effects. The exact boundary condition on the velocity potential ϕ at the linearized position of the free surface $z = 0$ is[14]

$$\frac{\partial^2\phi}{\partial t^2} = -g\frac{\partial\phi}{\partial z} + \frac{\sigma}{\rho}\frac{\partial}{\partial z}\left(\frac{\partial^2\phi}{\partial x^2} + \frac{\partial^2\phi}{\partial y^2}\right). \tag{9}$$

In the standard treatment of waves generated by floating bodies (see, e.g., Refs. 15–17), the surface-tension term is absent and two distinct limit cases arise according to whether the frequency of oscillation is smaller or greater than $(g/R)^{1/2}$, where R is the size of the body. In the first case Eq. (9) simplifies to $\partial\phi/\partial z = 0$, while in the second case it becomes $\phi = 0$. In the present situation the gravity term is always negligible and the oscillation frequency must be compared with $(\sigma/\rho R^3)^{1/2}$; when this quantity is small we again find $\phi \simeq 0$. We have already estimated the oscillation frequencies of a floating bubble in Sec. II. It is readily seen that this approximation is valid for the second mode [Eq. (16)], but not for the first mode [Eq. (5)]. An accurate treatment of this mode requires the inclusion of both inertial and surface-tension terms. This is unfortunate because the analysis then becomes considerably more involved and the greater effort required is out of proportion with the many simplifying assumptions introduced in the model. As already stated, our only purpose in this paper is to clarify the basic physics underlying the oscillations of a floating bubble. We therefore propose to make use only of the solution for ϕ obtained by imposing $\phi = 0$ on the undisturbed free surface $z = 0$. Our results will then be quantitatively correct for the volume mode which, as far as sound radiation in the water is concerned, is the important one. For the other (surface) mode, we can only expect to gain a qualitative understanding of its shape and an estimate of the order of magnitude of its frequency.

With this simplification the evaluation of the kinetic energy is reduced to the calculation of the following integral over the immersed surface of the bubble:

$$\mathscr{T} = \pi\rho R^2 \int_0^{\eta} \phi \frac{\partial\phi}{\partial n} \sin\theta\, d\theta, \tag{10}$$

where n is the unit normal into the bubble and the angle η is defined in Fig. 2. Evidently,

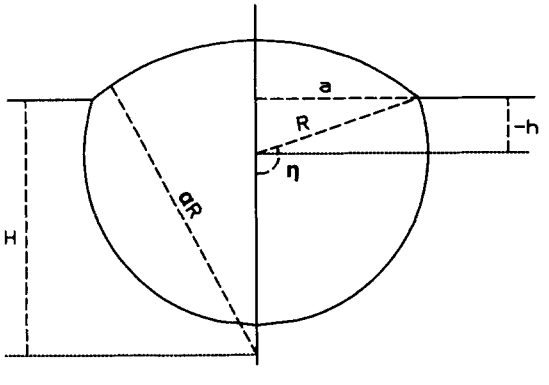

FIG. 2. The bubble model used in the present study.

$$\cos \eta = h/R \equiv \beta. \tag{11}$$

For a spherical segment with variable radius and vertical position we have

$$\frac{\partial \phi}{\partial n} = -\dot{R} + \dot{h} \cos \theta . \tag{12}$$

From the linearity of the problem for ϕ, we may then set

$$\phi = R(\dot{R}\phi_1 + \dot{h}\phi_2), \tag{13}$$

with which (10) takes the form

$$\mathcal{T} = \pi \rho R^3 [\dot{R}^2 F_1(\beta) + 2\dot{R}\dot{h}F_2(\beta) + \dot{h}^2 F_3(\beta)], \tag{14}$$

where

$$F_1 = -\int_0^\eta \phi_1 \sin\theta \, d\theta , \tag{15a}$$

$$F_2 = \frac{1}{2}\int_0^\eta (\phi_1 \cos\theta - \phi_2)\sin\theta \, d\theta , \tag{15b}$$

$$F_3 = \int_0^\eta \phi_2 \cos\theta \sin\theta \, d\theta . \tag{15c}$$

For the case of small oscillations, which is the only one we consider here, the value of $F_{j(\beta)}$, $j = 1,2,3$, can be calculated for the equilibrium position and kept constant: It does not seem possible to obtain a usable, closed form expression for these quantities except for the hemisphere case $\eta = \pi/2$ (see Appendix A); therefore, we have calculated them numerically using a boundary integral method. To give an idea of the accuracy of this numerical solution we may mention that for $\eta = \pi/2$, the exact solution of Appendix A gives $F_1 \simeq 0.4154$, $F_2 = -0.2500$, and $F_3 = 0.1667$, whereas the corresponding numerical results are $F_1 = 0.4166$, $F_2 = -0.2505$, and $F_3 = 0.1671$. The accuracy deteriorates somewhat when the bubble is nearly totally immersed, however. The functions F_j are plotted in Fig. 3 and tabulated in Table I.

For the potential energy $\mathcal{U}$ appearing in (8) we write

$$\mathcal{U} = \sigma S_l + 2\sigma S_u - \sigma\pi a^2 + \rho g V_l \bar{z} - \mathcal{U}_G, \tag{16}$$

where S_l and S_u are the surface areas of the lower and upper spherical segments given by

$$S_l = 2\pi R(R - h), \tag{17}$$

$$S_u = 2\pi\alpha R\{\alpha R - [(\alpha^2 - 1)R^2 + h^2]^{1/2}\}. \tag{18}$$

The upper spherical segment gives a contribution equal to twice its surface energy σS_u because it consists of two surfaces. The third term $\sigma\pi a^2$ in Eq. (16) is the surface energy

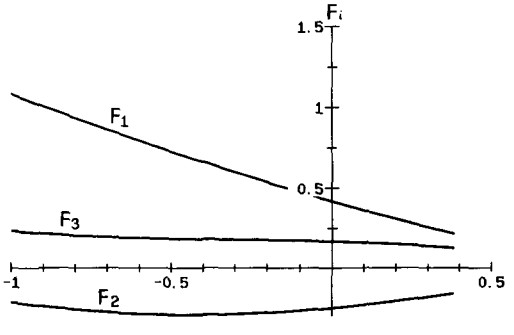

FIG. 3. Graphs of the functions F_1, F_2, and F_3 as defined in Eqs. (15).

TABLE I. The kinetic energy coefficients defined by (15) as a function of β, the normalized depth of immersion of the bubble defined by (11).

β	$F1$	$F2$	F_3
−0.995 00	1.081 84	−0.215 64	0.235 66
−0.900 00	1.008 25	−0.239 35	0.218 37
−0.800 00	0.935 05	−0.259 72	0.205 16
−0.700 00	0.864 07	−0.274 92	0.195 86
−0.600 00	0.794 93	−0.285 07	0.189 50
−0.500 00	0.727 52	−0.290 33	0.185 18
−0.400 00	0.661 80	−0.290 89	0.182 07
−0.300 00	0.597 78	−0.286 95	0.179 39
−0.200 00	0.535 52	−0.278 74	0.176 42
−0.100 00	0.475 07	−0.266 49	0.172 51
0.000 00	0.416 55	−0.250 50	0.167 07

of the hole of radius a created by the presence of the bubble on the undisturbed surface. Clearly,

$$a = (R^2 - h^2)^{1/2}. \tag{19}$$

The next to the last term in Eq. (16) is the potential of the buoyancy force given by the product of the immersed volume V_l,

$$V_l = (\pi/3)(R - h)^2(2R + h), \tag{20}$$

and the depth of its center of mass $\bar{z}$,

$$\bar{z} = (\pi/12V_l)(R - h)^3(3R + h). \tag{21}$$

The last term $\mathcal{U}_G$ in (16) is the $p\,dV$ energy stored in the bubble and is given by

$$\mathcal{U}_G = \int_{V_0}^{V} (p_G - p_0)dV, \tag{22}$$

where p_0 is the constant pressure outside the bubble, V_0 is the bubble equilibrium volume, and p_G is the internal pressure. The bubble volume V is the sum of the volumes of the lower and upper spherical segments,

$$V = V_l + V_u \tag{23}$$

and

$$V_u = (\pi/3)\{2\alpha^3 R^3 - [(\alpha^2 - 1)R^2 + h^2]^{1/2} \times [(2\alpha^2 + 1)R^2 - h^2]\}. \tag{24}$$

For simplicity we take an isothermal behavior

$$p_G = p_{G0} V_0/V, \tag{25}$$

since heat exchange across the thin upper surface is expected to be very efficient in preventing significant temperature differences. With this we find

$$\mathcal{U}_G = p_{G0} V_0 \log V/V_0 - p_0(V - V_0). \tag{26}$$

The viscous stresses, which counteract buoyancy and are ultimately responsible for the short-term stability of the surface bubble, do not appear explicitly in the formulation since, in the present model, they are an internal force acting in the upper spherical segment.

IV. EQUILIBRIUM STATE

By setting the partial derivatives of $\mathcal{U}$ with respect to α, R, and h equal to 0, we determine the equilibrium state of the system. In this way we find

$$\frac{\partial \mathcal{U}}{\partial \alpha} = \pi R\,[4\sigma - (p_G - p_0)\alpha R\,] \times\left(2\alpha R - \frac{(2\alpha^2-1)R^2 + h^2}{[(\alpha^2-1)R^2 + h^2]^{1/2}}\right), \tag{27}$$

from which, equating to 0, either $R = \pm h$ or

$$p_G - p_0 = 4\sigma/\alpha R. \tag{28}$$

The first condition with the plus sign, $R = h$, implies a geometry in which the immersed part of the bubble reduces to a point and is therefore unphysical; the minus sign corresponds to a bubble totally immersed and touching the surface. This configuration is a physical one in the absence of gravity effects (i.e., for very small bubbles); it will be shown to be actually included in (28) as a special case. Hence we retain only (28).

Proceeding similarly we find

$$\frac{\partial \mathcal{U}}{\partial R} = -(p_G - p_0)\pi R\left(2(\alpha^3+1)R - 2h - (2\alpha^2+1)H + \frac{\alpha^2 h^2}{H}\right) + 2\pi\sigma\left((4\alpha^2+1)R - h - 4\alpha H + \frac{2\alpha h^2}{H}\right) + \pi\rho g R(R-h)^2, \tag{29}$$

from which, by use of (28),

$$4(1-\beta) - 2(\alpha^2 - 1 + \beta^2)^{1/2} = \alpha(1-\beta)\,[1 + \tfrac{1}{2}\gamma(1-\beta)\,]. \tag{30}$$

Here the gravity parameter γ is defined as

$$\gamma = \rho g R^2/\sigma \tag{31}$$

and is seen to equal the square of the ratio ω_g/ω of the two frequencies defined in (1) and (3). Upon taking the derivative of (16) with respect to h we have

$$\frac{\partial \mathcal{U}}{\partial h} = \pi(R^2 - h^2)(p_G - p_0)\left(1 + \frac{h}{H}\right) - 2\pi\sigma \times\left(R - h + \frac{2\alpha R h}{H}\right) - \frac{\pi}{3}\rho g(R-h)^2(2R+h), \tag{32}$$

from which, again using (28),

$$2(1-\beta^2) - 2\beta(\alpha^2 - 1 + \beta^2)^{1/2} = \alpha(1-\beta)\,[1 + \tfrac{1}{6}\gamma(1-\beta)(2+\beta)\,]. \tag{33}$$

For the following developments it is useful to rewrite (30) and (33) in a different way. Elimination of $(\alpha^2 - 1 + \beta^2)^{1/2}$ leads to

$$\alpha = 2/[\,1 + \tfrac{1}{3}\gamma(1-\beta)\,], \tag{34}$$

while elimination of γ gives

$$(1 + \alpha/2)(1-\beta) = 2(\alpha^2 - 1 + \beta^2)^{1/2}.$$

This equation can be solved explicitly to express α as a function of β,

$$\alpha = \frac{2(1-\beta)^2 + 4[\,(1-\beta)(19 + 13\beta + \beta^2 - \beta^3)\,]^{1/2}}{(5-\beta)(3+\beta)}, \tag{35}$$

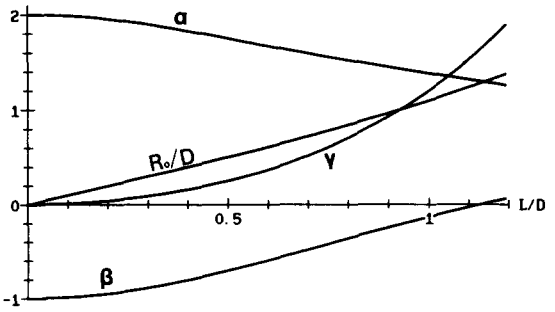

FIG. 4. The ratio of the cap radius to the radius of the immersed portion α, the ratio of the depth of the center of the lower spherical segment to its radius β, the gravity parameter γ, and the dimensionless radius of the lower spherical segment R/D, where D is the capillary length defined in (37), are shown as a function of the dimensionless radius of the equivalent sphere L/D.

and Eq. (34) can then be used to give $\gamma = \gamma(\beta)$. In this way both α and γ can be expressed as functions of the parameter β. An approximation valid for small bubbles, for which β is close to -1, is

$$\gamma = \tfrac{3}{4}(1+\beta), \quad \alpha = 1 - \beta.$$

If gravity is absent, so that $\gamma = 0$, $\alpha = 2$ and $\beta = -1$. In this case the bubble is totally immersed, tangent to the undisturbed surface, and the radius of curvature of the point of tangency is twice the radius of the immersed portion. The approximation $\alpha \simeq 2$ has been used by others in the past even for bubbles that were not totally immersed.[8] For $\gamma = 0.4077$ the lower surface is a hemisphere (i.e., $\beta = 0$) and $\alpha = 1.296$. The corresponding value of R for pure water in normal laboratory conditions would be 3.48 mm. We will argue later that the model is probably not reliable for such large bubbles.

At this point, given the amount of gas contained in the bubble, the geometry of the equilibrium state is completely determined in principle, although in practice the calculation is somewhat involved. To simplify the application of our results, we introduce a length L, which is the radius of a spherical bubble that would contain the same amount of gas as the floating bubble at the same internal pressure p_G:

$$L = (3V/4\pi)^{1/3}. \tag{36}$$

The length L can be related to the parameter R by the use of (20), (24), and the equilibrium relations (34) and (35). It is easy to see that the equilibrium configuration of the bubble in the present model can be described in terms of the single dimensionless parameter L/D, where D is a length characteristic of the fluid, the so-called *capillary length*, and is defined by

$$D = (\sigma/\rho g)^{1/2}. \tag{37}$$

The value of D for pure water in normal laboratory conditions is approximately 2.72 mm. In Fig. 4 we show graphs of R, α, β, and γ as functions of the dimensionless group L/D.

V. FORCE BALANCES

The preceding results are only formal and it is instructive to inquire to what extent they can be reproduced by

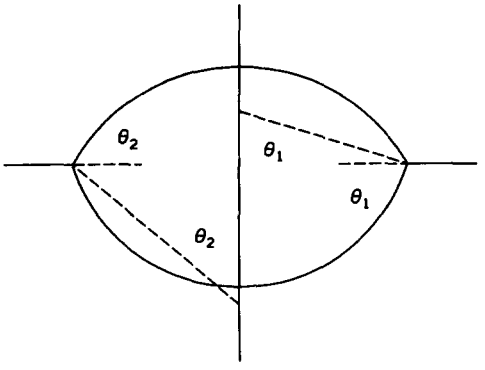

FIG. 5. Definition of the shape parameters used in Sec. V.

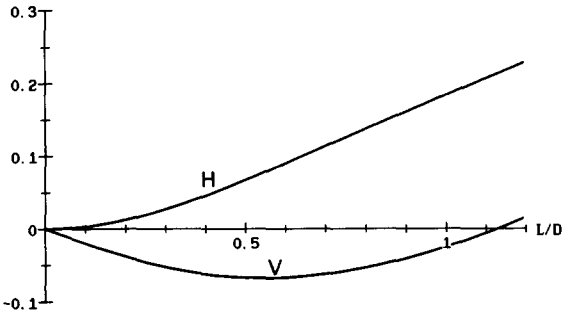

FIG. 6. The ratios of the spurious horizontal (line H) and vertical (line V) forces, necessary to turn the configuration of Fig. 1 into that of Fig. 2, to the magnitude $4\pi a\sigma \cos\theta_2$ of the horizontal force acting on the contact line.

force-balance arguments. In this way some insight will also be gained on the domain of validity of the model.

The total force acting on the upper cap of the bubble in the vertical direction consists of the pressure forces $\pi a^2 p_G$ and $-\pi a^2 p_0$ and the surface-tension force $2\times 2\pi a\sigma \sin\theta_2$ (see Fig. 5 for the definition of the symbols). Since $\sin\theta_2 = a/\alpha R$, balancing these forces leads to

$$\pi a^2(p_G - p_0) = 4\sigma\pi a \cdot a/\alpha R, \tag{38}$$

which is easily seen to coincide with (28). The same result can be obtained by adding the Laplace pressures of the two interfaces which make up the bubble's cap.

Before applying a similar argument to the lower spherical segment, it must be realized that the natural equilibrium condition of a floating bubble is closer to that sketched in Fig. 1 than to the one of Fig. 2 which we have imposed on the Lagrangian. As already noted, in order to have the configuration of Fig. 2, we must therefore presuppose the existence of an extra force f_v, the magnitude of which can actually be determined by writing the analog of the force balance (38) for the lower spherical segment:

$$-\pi a^2(p_G - p_0) + \rho g V_l + 2\pi a\sigma \sin\theta_1 + f_V = 0,$$

where the angle θ_1 is defined in Fig. 5. Elimination of $p_G - p_0$ by use of (28) and α by use of (34) leads to

$$f_V = (\pi/3)\rho g h(R-h)^2. \tag{39}$$

This force is negative, i.e., it acts downward if the bubble is more than half immersed ($h<0$, see Fig. 2), which, as will be shown, is necessary for our model to be valid. From a comparison of Figs. 1 and 2 the sign of f_V is therefore as expected.

In a similar fashion, the horizontal force balance at the points of the ring where the three surfaces come together gives

$$2\pi\sigma a(1 - 2\cos\theta_2 - \cos\theta_1) + f_H = 0,$$

where f_H is the additional horizontal force necessary to give the configuration of Fig. 2. Proceeding as before we find

$$f_H = 4\pi a\sigma[(2-\alpha)/(2+\alpha)]\cos\theta_2.$$

Since $\alpha \sim 2$ when the bubble is small and therefore nearly totally immersed, we see that this force is small for small bubbles: It is also clearly positive, which agrees with what is needed to transform the configuration of Fig. 1 into that of Fig. 2.

Our results can be expected to apply to a real floating bubble only if the artificial forces f_V and f_H are small. In Fig. 6 we show graphs of the ratio of these forces to $4\pi a\sigma \cos\theta_2$. The reason for using the magnitude of a horizontal force also to judge the relative importance of the vertical fictitious force is that for a very small bubble, which is nearly totally immersed, all the vertical forces are very small, so that the presence or absence of f_V is immaterial.[18] As L/D increases from 0 the biggest error is seen to be associated with the vertical force balance. The line marked V in Fig. 6 crosses the level of 5% for $L/D = 0.281, \beta = -0.899$. This seems to be a reasonable upper limit for the reliability of the present model. The corresponding value of L for water is 0.763 mm.

The question of the limits of validity of our model can be examined from an alternative point of view. It is a matter of common experience that large floating bubbles tend to be only slightly immersed and to have a hemispherical cap.[13] The equilibrium configuration of such a bubble can readily be estimated if the immersed part is taken to be essentially flat. If d is the depth of immersion of the base, the excess internal pressure due to surface tension must balance the hydrostatic head, so that $4\sigma/R_c \simeq \rho g d$, where R_c is the cap radius. From this we have $d/R_c \simeq (2D/R_c)^2$. This model presupposes that $d \ll R_c$ and therefore that $D \ll R_c$. The transition between the configuration of Figs. 1 or 2 and that with a flat base can therefore be expected to take place for $R_c \sim D$. One can infer that the validity of our model is restricted to the opposite limit case of $R \ll D$ or, equivalently, $L \ll D$: this is consistent with the estimate previously given in Sec. II.

VI. NORMAL MODES

Since the kinetic energy is independent of the radius of the bubble cap, the Lagrange equation of motion for the variable α reduces to

$$\frac{\partial \mathcal{U}}{\partial \alpha} = 0,$$

which implies that the relation expressed by Eq. (28) is satisfied throughout the motion. By use of this relation α can be expressed in terms of R and h and the number of dynamical variables reduced by one. If we set

$$R = R_0(1+X), \quad h = h_0(1+Y), \tag{40}$$

Lagrange's equations, to lowest order, take the form

$$A\frac{d^2}{dt^2}\begin{vmatrix}X\\Y\end{vmatrix}+\omega^2 B\begin{vmatrix}X\\Y\end{vmatrix}=0, \tag{41}$$

where the frequency ω has been defined in (1) and, here and in the following, the index 0 indicates equilibrium values. In (41) A and B are matrices given by

$$A=\begin{vmatrix}F_1 & \beta_0 F_2\\ F_2 & \beta_0 F_3\end{vmatrix}, \tag{42}$$

$$B=\begin{vmatrix}a_{11} & \beta_0 a_{12}\\ a_{12} & \beta_0 a_{22}\end{vmatrix}. \tag{43}$$

The functions F_j defined in (15) are to be evaluated at β_0, as already noted. The matrix elements of B are complicated expressions involving α, β, γ, and the dimensionless parameter

$$K=p_{G0}R/2\sigma, \tag{44}$$

which is clearly related to the ratio ω_V/ω between the frequencies defined in (1) and (2). The expressions for these matrix elements of B are given in full in Appendix B. Here we show only the asymptotic forms valid for $\gamma\to 0$:

$$a_{11}=12K-\tfrac{7}{2}-(8K-\tfrac{7}{6})\gamma, \tag{45}$$

$$a_{12}=\tfrac{1}{2}-(4K+\tfrac{5}{6})\gamma, \tag{46}$$

$$a_{22}=\tfrac{1}{2}-\tfrac{1}{6}\gamma. \tag{47}$$

The approximations (45)–(47) are formally correct for small γ provided that $K=O(1)$ or, more precisely, provided that $K\gamma^2\ll\gamma$. This circumstance severely limits their accuracy since in practice K is typically very large. The exact expressions have been used in the numerical results to be shown in Secs. VII and VIII.

The general solution of (41) may be written as

$$\begin{vmatrix}X\\Y\end{vmatrix}=\begin{vmatrix}X_1\\1\end{vmatrix}u_1^{\pm}e^{\pm i\omega\lambda_1 t}+\begin{vmatrix}X_2\\1\end{vmatrix}u_2^{\pm}e^{\pm i\omega\lambda_2 t}, \tag{48}$$

where $u_1^{\pm}$ and $u_2^{\pm}$ are complex constants depending on the initial conditions and λ_1, λ_2, which may be regarded as dimensionless oscillation frequencies, are given by the relation

$$\det(B-\lambda_j^2 A)=0,\quad j=1,2,$$

or, more explicitly,

$$\lambda_{1,2}^2=\frac{a_{11}F_3+a_{22}F_1-2a_{12}F_2}{2(F_1F_3-F_2^2)}\times\left[1\pm\left(1-\frac{4(F_1F_3-F_2^2)(a_{11}a_{22}-a_{12}^2)}{(a_{11}F_3+a_{22}F_1-2a_{12}F_2)^2}\right)^{1/2}\right]. \tag{49}$$

The vectors $V_j^T=|X_j\ 1|^T, j=1,2$, in (41) are (arbitrarily normalized) eigenvectors of the problem $(B-\lambda^2 A)V_j=0$.

In Figs. 7 and 8 we show a plot of λ_1 and λ_2 as a function of L/D for several values of the parameter Π defined by

$$\pi\equiv\gamma^{-1/2}(K-2/\alpha)=p_0/2\sqrt{\sigma\rho g}. \tag{50}$$

The curves are smooth except for very small values of L/D, which is a consequence of the already mentioned poor accuracy of the boundary element calculation of the kinetic energy coefficients (15) when the bubble is nearly totally immersed.

A striking feature that emerges from the comparison between Figs. 7 and 8 is the large difference in the orders of magnitude of the two frequencies. For reasons that will be clear below, we call the mode of Fig. 7, for which λ_1 is of order unity, the *surface mode* and that of Fig. 8, for which λ_2 is large, the *volume mode*. Other features of the normal modes are shown in Figs. 9–11. Figure 9 is a graph of the normalized radial changes X_1 and X_2 as a function of L/D. These results, which essentially give the shape of the normal modes, are seen to be relatively insensitive to the variation of the parameter Π over two orders of magnitude. Figures 10 and 11 show the amplitudes of the changes of the lower and upper volumes V_l and V_u for the cases of air and water at normal pressure, for which $\Pi\simeq 1871$. These amplitudes are relative and with respect to a unit change in the normalized depth h. In other words, the quantity plotted is

$$\Delta_s=\frac{h}{V_s}\left(\frac{dV_s}{dh}\right)_j=\frac{h}{V_s}\left[\left(\frac{\partial V_s}{\partial R}\right)_h\left(\frac{dR}{dh}\right)_j+\left(\frac{\partial V_s}{\partial h}\right)_R\right],\quad j=1,2,\quad s=l,u, \tag{51}$$

where $(dR/dh)_j$ is computed for the jth normal mode. With the aid of Figs. 9–11 we can now elucidate the physics of the process.

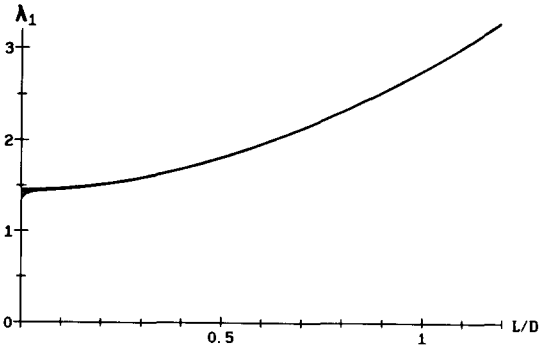

FIG. 7. The eigenvalue λ_1 (the dimensionless frequency of the surface mode) as a function of the dimensionless bubble size L/D. Three nearly indistinguishable curves corresponding to the values 200, 1871, and 20 000 of the stiffness parameter Π defined in (50) are shown.

VII. THE SURFACE MODE

All the quantities pertaining to the smaller value of λ carry the index 1. In the range of validity of the present

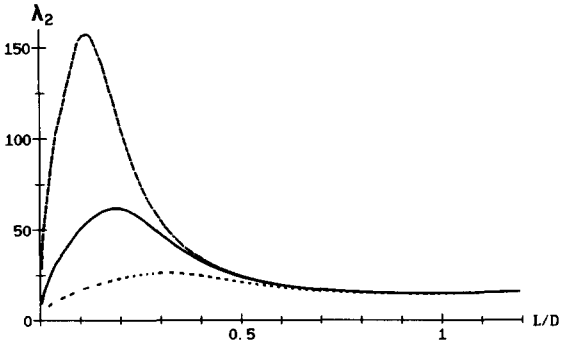

FIG. 8. The eigenvalue λ_2 (the dimensionless frequency of the volume mode) as a function of the dimensionless bubble size L/D for the values 200 (dotted line), 1871 (solid line), and 20 000 (dashed line) of the stiffness parameter π defined in (50).

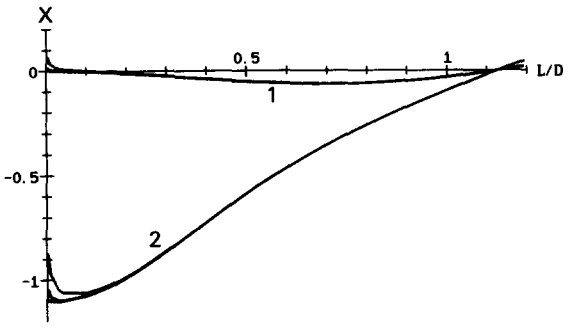

FIG. 9. The eigenvectors corresponding to the two modes of oscillations for $\Pi = 200$, 1871, and 20 000. The lines may be interpreted as giving the relative change of the radius of the lower spherical segment for a unit relative change of the depth of its center. Recall that this quantity is negative in the range of validity of the model.

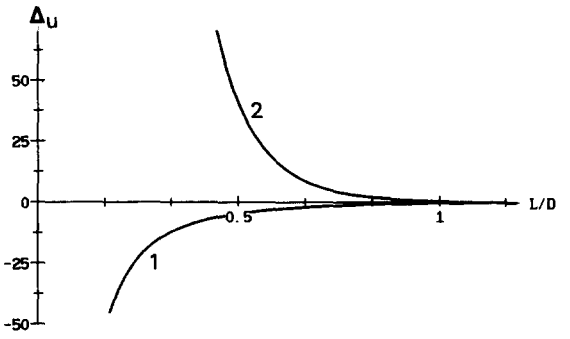

FIG. 11. The relative change of the volume of the bubble cap for a unit relative change of the depth of submergence of the center of the immersed spherical segment, see Eq. (51). Here $\Pi = 1871$.

model the bubble is more than half-immersed and therefore $h_0 < 0$. In Fig. 12 we show a drawing of the equilibrium configuration of a bubble with $L/D = 0.282$ (dashed line) and its shape in mode-1 oscillation (solid line). Using the fact that in the eigenvalue equation (49) the second term in the square root is typically much smaller than 1 we have, approximately,

$$\lambda_1^2 \simeq (a_{11}a_{22} - a_{12}^2)/(a_{11}F_3 + a_{22}F_1 - 2a_{12}F_2) \qquad (52)$$

or, since both a_{12} and a_{22} are typically smaller than a_{11},

$$\lambda_1^2 \simeq a_{22}/F_3. \qquad (53)$$

From Fig. 7 and Eq. (47) the result (53) is seen to be a positive number of order 1, so that the dimensional frequency of this mode is of the order of ω, in agreement with the estimate (5) previously given.

From the analysis of Figs. 9–11 the mechanics of the surface mode can be described as follows. Suppose that h increases, so that the bubble is less immersed (recall that $h_0 < 0$). This causes but a slight increase in the radius of curvature R of the lower hemisphere (Fig. 9), a modest contraction of the volume of the lower spherical segment (Fig. 10), and a large increase of the upper volume (Fig. 11). However, since in this size range most of the bubble volume is immersed, the increase of the total volume is negligible. As a consequence, the frequency is essentially independent of the compressibility of the bubble, measured by the parameter Π defined in (50), in agreement with Fig. 7, in which the three lines corresponding to $\Pi = 200$, 1871, and 20 000 are practically superposed.

As a result of the small change of the immersed volume, as a sound source in the liquid, the surface mode would behave as a dipole, although the pressure-release boundary condition turns it into a quadrupole. The radiated noise is therefore negligible. However, the cap volume increases substantially and therefore, in air, the oscillating bubble behaves very nearly as a monopole.

As already remarked, the approximation $\phi \simeq 0$ on the free surface is not really justified for the surface mode. We can therefore claim little more than to have elucidated its main qualitative features. To the extent that these features correspond to what can be inferred from dimensional analysis, this claim appears to be justified.

VIII. THE VOLUME MODE

In Fig. 12 the dashed-and-dotted line indicates the shape of the bubble in mode-2 oscillation. Note that the radius of curvature of the upper surface is so large as to appear nearly flat. The nature of this mode is strikingly different from that of the surface mode in that the volume of the bubble undergoes substantial changes. From Fig. 9 it is seen that the amplitude of oscillation of the radius and depth of immersion are comparable, at least for small bubbles, and from Figs. 10 and 11 that both the lower and upper volumes

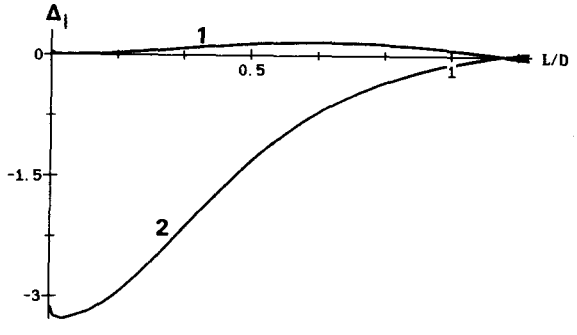

FIG. 10. The relative change of the volume of the submerged portion of the bubble for a unit relative change of the depth of submergence of its center, see Eq. (51). Here $\Pi = 1871$.

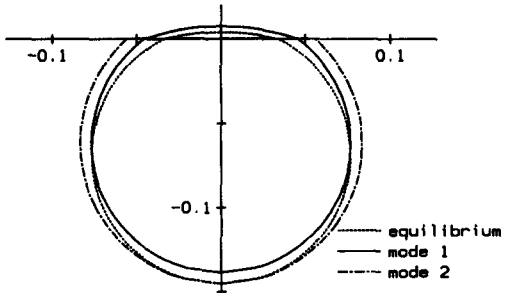

FIG. 12. Shape of the normal modes for $\Pi = 1871$. The dashed line indicates the equilibrium configuration of a bubble with $L/D = 0.2820$, $R/D = 0.2823$, $\beta = -0.8980$, $\alpha = 1.904$, and $\gamma = 0.079\,72$. The corresponding value of L in water is 0.7683 mm. The solid line indicates the shape of the mode-1 (surface) oscillation. The dashed-and-dotted line shows the shape of the mode-2 (volume) oscillation. Note that for the volume mode the upper radius of curvature has grown so large that the cap is nearly flat.

change appreciably. For the eigenvalue λ_2 the approximate expression analogous to (52) is

$$\lambda_2^2 \simeq (F_1 a_{22} + F_3 a_{11} - 2F_2 a_{12})/2(F_1 F_3 - F_2^2) \tag{54}$$

and the analog of (53) is

$$\lambda_2^2 \simeq [F_3/(F_1 F_3 - F_2^2)]a_{11}. \tag{55}$$

By use of (1), (44), and (45) we find a corresponding dimensional frequency given by

$$\{6[F_3/(F_2^2 - F_1 F_3)](p_{G0}/R_0^2 \rho)\}^{1/2}, \tag{56}$$

in agreement with the previous estimate (6). It can be appreciated from Fig. 7 that this frequency is orders of magnitude larger than that of the surface mode. A consequence is that the wavelength of the ripples produced on the free surface is small compared with R and therefore the criterion for the validity of the approximate boundary condition $\phi \sim 0$ is amply met. We therefore expect our theory to be quantitatively accurate for the volume oscillations of sufficiently small bubbles.

In view of the relatively large volume increase of the submerged portion, a bubble oscillating in the volume mode behaves as an acoustic monopole source in the water, with the net effect of a dipole due to the pressure-release boundary condition. The cap volume also undergoes substantial changes, so that the volume mode is a monopole source in air, just as is the surface mode.

IX. CONCLUSIONS

On the basis of a simplified model for the dynamics of a floating bubble we have found that two very different modes of oscillations exist. The restoring force of the *volume mode* is provided mainly by the expansion and compression of the gas contained in the bubble and has a frequency with the same order of magnitude as that of a spherical bubble in an unbounded liquid. On the other hand, in the case of the *surface mode* the restoring force is essentially surface tension. The surface mode has a much smaller frequency than the volume mode comparable to the frequency of fixed-volume shape oscillations of a spherical bubble in an infinite liquid. These conclusions are borne out by dimensional considerations. In view of the approximations introduced, our analysis is correct for the volume mode, but can only predict the existence and broad characteristics of the surface mode.

As far as sound radiation in the water is concerned, the surface mode has a quadrupole nature, while the volume mode has a dipole character. The volume mode is therefore a much more efficient source of sound; however, its large frequency indicates a strong restoring force, making it hard to excite. For radiation in air both modes behave as monopoles and the softer surface mode will be easy to excite. When two surface bubbles coalesce, the excess surface energy gives rise to oscillations. Our results lead one to expect a much stronger noise in the air than in the water, a conclusion that is borne out by qualitative experiments conducted by Pumphrey.[7]

ACKNOWLEDGMENTS

The authors are grateful to H. C. Pumphrey for making available to them the results of his experiments.

This study was supported by the Underwater Acoustics Division of the Office of Naval Research.

APPENDIX A: KINETIC ENERGY COEFFICIENTS FOR A HALF-IMMERSED SPHERE

The solutions of Laplace's equation defined in (13) and vanishing on the free surface are, for $h = 0$ (i.e., $\eta = \pi/2$),

$$\phi_1 = \sum_{k=0}^{\infty} (-1)^{k+1} \frac{(2k-1)!!}{2^{k+2} k!} \frac{4k+3}{(k+1)^3} \times \left(\frac{R}{r}\right)^{2(k+1)} P_{2k+1}(\cos\theta)$$

and

$$\phi_2 = (R^2/2r^2)\cos\theta.$$

With these results it is easy to show that

$$F_1(0) = \sum_{k=0}^{\infty} \frac{4k+3}{2^{2k+3}(k+1)^3} \left(\frac{(2k-1)!!}{k!}\right)^2 \simeq 0.415\,43,$$

while $F_2(0) = -\frac{1}{4}$ and $F_3(0) = \frac{1}{6}$.

APPENDIX B: ELEMENTS OF THE MATRIX

We give here the explicit form of the coefficients a_{ij} which appear in expression (43) of the "mass" matrix B:

$$a_{11} = \mathcal{U}_{RR} - \mathcal{U}_{\alpha R}^2/\mathcal{U}_{\alpha\alpha}, \tag{B1}$$

$$a_{12} = \mathcal{U}_{Rh} - \mathcal{U}_{\alpha R}\mathcal{U}_{\alpha h}/\mathcal{U}_{\alpha\alpha}, \tag{B2}$$

$$a_{22} = \mathcal{U}_{hh} - \mathcal{U}_{\alpha h}^2/\mathcal{U}_{\alpha\alpha}, \tag{B3}$$

where we have used the notation

$$\mathcal{U}_{xy} = \frac{K}{\pi R V}\frac{\partial V}{\partial x}\frac{\partial V}{\partial y} - \frac{2}{\alpha\pi R}\frac{\partial^2 V}{\partial x\,\partial y} + \frac{\partial^2 S}{\partial x\,\partial y} + \frac{\gamma}{2\pi R^2}\frac{\partial^2 (V_l \bar{z})}{\partial x\,\partial y},$$

in which x, y stand for any one of the dynamical variables R, h, and α. Furthermore,

$$S = (1/2\pi)[(S_l + 2S_u) - \tfrac{1}{2}(R^2 - h^2)],$$

and S_l, S_u, V_l, and $\bar{z}$ are defined in (17), (18), (20), and (21). The explicit forms of the derivatives appearing in (B1)–(B3) are

$$\frac{1}{\pi R}\frac{\partial^2 V}{\partial R^2} = 4(\alpha^3 + 1) - 2\beta - \frac{(\alpha^2-1)(2\alpha^2+1)(2\alpha^2-2+3\beta^2) + (\alpha^2+1)\beta^4}{(\alpha^2-1+\beta^2)^{3/2}},$$

$$\frac{1}{\pi R}\frac{\partial^2 V}{\partial h^2} = 2\beta - \frac{(\alpha^2-1)(1-3\beta^2) - 2\beta^4}{(\alpha^2-1+\beta^2)^{3/2}},$$

$$\frac{1}{\pi R^3}\frac{\partial^2 V}{\partial \alpha^2} = 4\alpha - \frac{4\alpha^4 - 6\alpha^2 + 1 + 6\alpha^2\beta^2 - 2\beta^2 + \beta^4}{(\alpha^2-1+\beta^2)^{3/2}},$$

$$\frac{1}{\pi R}\frac{\partial^2 V}{\partial R\,\partial h}=-\left(2+\beta\frac{\alpha^2-1+(\alpha^2+1)\beta^2}{(\alpha^2-1+\beta^2)^{3/2}}\right),$$

$$\frac{1}{\pi R^2}\frac{\partial^2 V}{\partial \alpha\,\partial R}=\alpha\left(6\alpha-\frac{6\alpha^4-9\alpha^2+3+9\alpha^2\beta^2-5\beta^2+2\beta^4}{(\alpha^2-1+\beta^2)^{3/2}}\right),$$

$$\frac{1}{\pi R^2}\frac{\partial^2 V}{\partial \alpha\,\partial h}=\frac{\alpha\beta(1-\beta^2)}{(\alpha^2-1+\beta^2)^{3/2}},$$

$$\frac{1}{\pi R^2}\frac{\partial V}{\partial R}=2(\alpha^3+1)-2\beta-\left(\frac{(\alpha^2-1)(2\alpha^2+1)+(\alpha^2+1)\beta^2}{(\alpha^2-1+\beta^2)^{1/2}}\right),$$

$$\frac{1}{\pi R^2}\frac{\partial V}{\partial h}=(1-\beta^2)\left(1+\frac{\beta}{(\alpha^2-1+\beta^2)^{1/2}}\right),$$

$$\frac{1}{\pi R^3}\frac{\partial V}{\partial \alpha}=\alpha\left(2\alpha-\frac{2\alpha^2-1+\beta^2}{(\alpha^2-1+\beta^2)^{1/2}}\right),$$

$$\frac{\partial^2 S}{\partial R^2}=1+2\alpha\left(2\alpha-(\alpha^2-1)\frac{2(\alpha^2-1)+3\beta^2}{(\alpha^2-1+\beta^2)^{3/2}}\right),$$

$$\frac{1}{R^2}\frac{\partial^2 S}{\partial \alpha^2}=2\left(2-\frac{\alpha(2\alpha^2-3+3\beta^2)}{(\alpha^2-1+\beta^2)^{3/2}}\right),$$

$$\frac{\partial^2 S}{\partial h^2}=1-2\alpha\frac{\alpha^2-1}{(\alpha^2-1+\beta^2)^{3/2}},$$

$$\frac{\partial^2 S}{\partial R\,\partial h}=-\left(1+\frac{2\alpha\beta^3}{(\alpha^2-1+\beta^2)^{3/2}}\right),$$

$$\frac{1}{R}\frac{\partial^2 S}{\partial \alpha\,\partial R}=2\left(4\alpha-\frac{4\alpha^4-6\alpha^2+2+6\alpha^2\beta^2-3\beta^2+\beta^4}{(\alpha^2-1+\beta^2)^{3/2}}\right),$$

$$\frac{1}{R}\frac{\partial^2 S}{\partial \alpha\,\partial h}=\frac{2\beta(1-\beta^2)}{(\alpha^2-1+\beta^2)^{3/2}}.$$

All these expressions must be evaluated for the equilibrium conditions.

[1]W. D. Garrett, Deep Sea Res. **14**, 661 (1967).
[2]J. J. Bikerman, J. Appl. Chem. **18**, 266 (1968).
[3]Q. A. Zhang, V. Klemas, and Y.-H. L. Hou, J. Geophys. Res. **88**, 701 (1983).
[4]S. R. Burger and D. C. Blanchard, J. Geophys. Res. **88**, 7724 (1983).
[5]J. P. Chen, P. S. Hahn, and J. C. Slattery, AIChE J. **30**, 622 (1984).
[6]P. S. Hahn, J. D. Chen, and J. C. Slattery, AIChE J. **31**, 2026 (1985).
[7]H. Pumphrey (private communication).
[8]M. M. Nicolson, Proc. Cambridge Philos. Soc. **45**, 288 (1949).
[9]D. C. Blanchard and A. H. Woodcock, Tellus **9**, 145 (1957).
[10]F. J. Resch, J. S. Darrozes, and G. M. Afeti, J. Geophys. Res. **91**, 1019 (1986).
[11]H. Lamb, *Hydrodynamics* (Cambridge U.P., Cambridge, 1932; Dover, New York, 1945), 6th ed., p. 473.
[12]M. S. Plesset and A. Prosperetti, Annu. Rev. Fluid Mech. **9**, 145 (1977).
[13]H. M. Princen, J. Colloid Sci. **18**, 178 (1963).
[14]L. L. Landau and E. M. Lifshitz, *Fluid Mechanics* (Pergamon, New York, 1959), Chap. 7.
[15]F. Ursell, Proc. R. Soc. London Ser. A **220**, 90 (1953).
[16]T. F. Ogilve, in *Advances in Applied Mechanics*, edited by C. S. Yih (Academic, New York, 1977), Vol. 17, p. 92.
[17]A. Hulme, J. Fluid Mech. **121**, 443 (1982).

[18]To gauge the magnitude of f_v against the true vertical forces one could use either the pressure or surface-tension forces appearing in the vertical force balance. If, for instance, the surface-tension force is used, we find $|f_v/2\pi\theta\sin\theta_1|\ll 1$. This ratio is readily seen to equal $\frac{1}{3}\gamma|\beta|(1-\beta)/(1+\beta)$. As the bubble gets smaller, $\gamma\to 0$ and $\beta\to -1$. It is easy to prove that the limit of this ratio as $R\to 0$ has the value $\frac{2}{3}$, which is not very small. However, this argument would be misleading for the reason stated in the text.